Modified cyclodextrin-based nanoparticles mediated delivery of siRNA for Huntingtin gene silencing across an *in vitro* BBB model

Monique C. P. Mendonça[1], Michael F. Cronin[1], John F. Cryan[2], Caitriona M. O'Driscoll[1*]

[1]Pharmacodelivery Group, School of Pharmacy, University College Cork, Ireland

[2]APC Microbiome Ireland, University College Cork, Cork, Ireland; Department of Anatomy and Neuroscience, University College Cork, Cork, Ireland.

Submitted to: European Journal of Pharmaceutics and Biopharmaceutics

*Corresponding author

Prof. Caitriona O'Driscoll. School of Pharmacy, Cavanagh Pharmacy Building, College Rd, University College Cork, T12 YT20, Cork, Ireland; e-mail: caitriona.odriscoll@ucc.ie

Abstract

Huntington's disease (HD) is a neurodegenerative disorder caused by a mutation in the huntingtin (*HTT*) gene, leading to a toxic version of the HTT protein. There are currently no disease-modifying therapies available. In this scenario, gene-based treatments for HD aimed at lowering HTT levels have become one of the most promising emerging therapeutic options. To date, however, promising results have only been achieved following direct intrathecal or intracranial injections designed to circumvent the blood-brain barrier (BBB). Consequently, efforts to develop less invasive delivery platforms are highly desirable. Here, we described a novel delivery system based on modified cyclodextrin nanoparticles (CDs) loaded with small interfering RNAs (siRNAs) targeting *HTT* and complexed with the rabies virus glycoprotein (RVG), a BBB-shuttle peptide. Results using an *in vitro* BBB model, indicate the formulation successfully crosses the brain endothelial cells, releases the encapsulated siRNAs into the cytoplasm of neuronal cells, and mediates downregulation of HTT. In conclusion, the CD platform is a promising option for delivery of siRNA-based therapeutics for HD with wider potential to treat other diseases with a genetically validated target in the central nervous system.

Keywords: Huntington’s disease; nanocarriers; non-viral gene therapy, RVG, targeted cyclodextrins

1. Introduction

Huntington's disease (HD) is an autosomal dominant neurodegenerative disease caused by an abnormal expansion of a CAG repeat in the huntingtin (*HTT*) gene, which translates as a mutant HTT (mHTT) protein containing an elongated polyglutamine (PolyQ) stretch at the N-terminal region. PolyQ expansions trigger both HTT protein loss-of-function and toxic gain-of-function effects, thereby leading to neuronal death and ultimately contributing to the gradual progression of motor, cognitive, and psychiatric symptoms [1,2]. Currently, there are no approved disease-modifying therapies for the treatment of HD, and only palliative therapies exist.

As a genetic disease, genetic therapies targeting HTT DNA, mRNA, and protein have emerged as potential disease-modifying treatments for HD. These approaches aim to reduce mHTT levels - the prime cause of HD - by either modulating gene transcription and translation or by direct modification of the mutated gene (genome editing) [3]. Therapeutics strategies designed to interact with *HTT* DNA include zinc-finger nucleases (ZFNs), transcription activator-like effector nucleases (TALENs), and Cas9 or other RNA-guided bacterial nucleases. At the post-transcriptional level, methods that interact directly with *HTT* mRNA include RNA interference (*e.g* small interfering RNAs (siRNAs)) and antisense oligonucleotides (ASOs) [3,4]. However, due to the unfavorable physicochemical properties of RNA molecules and the subsequent challenges for systemic administration, these therapies have been administered directly into the brain or cerebrospinal fluid [5], which can cause the patient discomfort and also carry the risks of complications from highly invasive neurosurgery [6]. Therefore, efforts to develop less invasive delivery platforms are highly desirable.

Delivery to the brain following systemic administration, also an option for HD, remains a major challenge due to the presence of the blood-brain barrier (BBB). The BBB

is a complex multicellular structure formed by endothelial cells, pericytes, astrocytes, and neurons that separates the central nervous system (CNS) from the peripheral blood circulation. In order to maintain the CNS homeostasis, the BBB tightly controls the passage of molecules and ions in and out of the brain, as well as protecting the brain from toxins, pathogens, and other xenobiotic molecules. However, the BBB also prevents most therapeutic molecules from entering the brain, thus, limiting the treatment of several neurological disorders [7]. To overcome this limitation, nanotechnology-based approaches have been developed. Among a diversity of nanomaterials, the efficiency of cyclodextrins (CDs) as favorable delivery platforms for gene therapy has been well recognized [5,8,9].

CDs are a family of natural, biodegradable, and biocompatible cyclic oligosaccharides with a hydrophilic exterior surface and a hydrophobic cavity. This structure is responsible for their ability to act as molecular containers encapsulating hydrophobic guests inside their cavities [10]. Moreover, the potential of CDs to improve the solubility and dissolution rate, physicochemical stability, bioavailability, permeability, and intensity or duration of therapeutic activity of existing and emerging drugs candidates has been described [11]. Previously, we demonstrated that various functionalised CDs successfully delivered siRNA and induced silencing of the target gene in prostate cancer cell lines [12,13], acute myeloid leukemia cells [14] and glioblastoma cells [15]. Sustained knockdown effects and alleviation of motor deficits were also observed in the striatum of the R6/2 mouse, a model of HD, following direct injection of the modified amphiphilic CDs delivering *HTT* targeted siRNAs into the brain [16].

The aim of the present study was to develop a novel delivery system that could deliver siRNA cargo into target CNS diseased cells. To achieve this, we designed

chemically modified CDs-based nanoparticles (NPs) loaded with siRNA against human *HTT* targeted with rabies virus glycoprotein (RVG), a BBB shuttle peptide. RVG complexes primarily bind to nicotinic acetylcholine receptors (nAChR) expressed by brain endothelial cells and neuronal cells, and thus permeate the BBB by receptor-mediated transcytosis [17]. The cellular uptake and silencing efficacy of the CDs NPs were evaluated in an *in vitro* co-culture BBB model of HD incorporating the human cerebral microvascular endothelial cell line (hCMEC/D3) in combination with the rat striatal embryonic neuronal cell line ST14A which expresses the full-length human HD gene [18].

2. Materials and Methods

2.1 Materials

The RVG peptide was purchased from GenScript Biotech (Leiden, The Netherlands). *HTT* target siRNA (sense strand ′5GCUCAUCAUUAGUAAAAAUGACtt3′) was obtained from Thermo Fisher Scientific (Massachusetts, USA). Non-silencing siRNA (sense strand, 5′-UUCUCCGAACGUGUCACGUdTdT-3′) and FAM-labeled siRNA (sense strand, 5′-[6FAM] UUCUCCGAACGUGUCACGUdTdT-3) were purchased from Sigma Aldrich (Wicklow, Ireland). EBM-2 endothelial cell growth basal medium and EGM-2 Endothelial SingleQuots Kit™ were purchased from Lonza (Slough, UK). Mouse monoclonal antibody against Huntingtin protein (MAB2166) was purchased from MilliporeSigma, whereas Alexa 488-conjugated goat anti-mouse IgG (A-11001) was received from Invitrogen (Thermo scientific, Massachusetts, USA). Rabbit polyclonal antibody against Zonula Occludens (ZO1) (#21773) was purchased from ProteinTech (Thermo scientific, Massachusetts, USA), while mouse anti-rabbit IgG-CFL 488 (sc-

516248) was obtained from Santa Cruz Biotechnology (Dallas, USA). Primers were purchased from Eurofins Genomics (Glanmire, Ireland) and SensiFAST™ SYBR® Lo-Rox from Bioline (Luckenwalde, Germany). All other chemicals and materials were of analytical grade and purchased from Sigma-Aldrich.

2.2 Synthesis of cyclodextrin-siRNA complexes

The synthesis of cationic amphiphilic CDs has been previously reported [19, 20]. In this work a change in the amino group was introduced in order to decrease the pK_a below 7 (Scheme 1). The final product was reconstituted with RNAse-free water (0.25 mg/mL) and mixed with a solution of siRNA at a mass ratio of CDs:siRNA of 10:1.

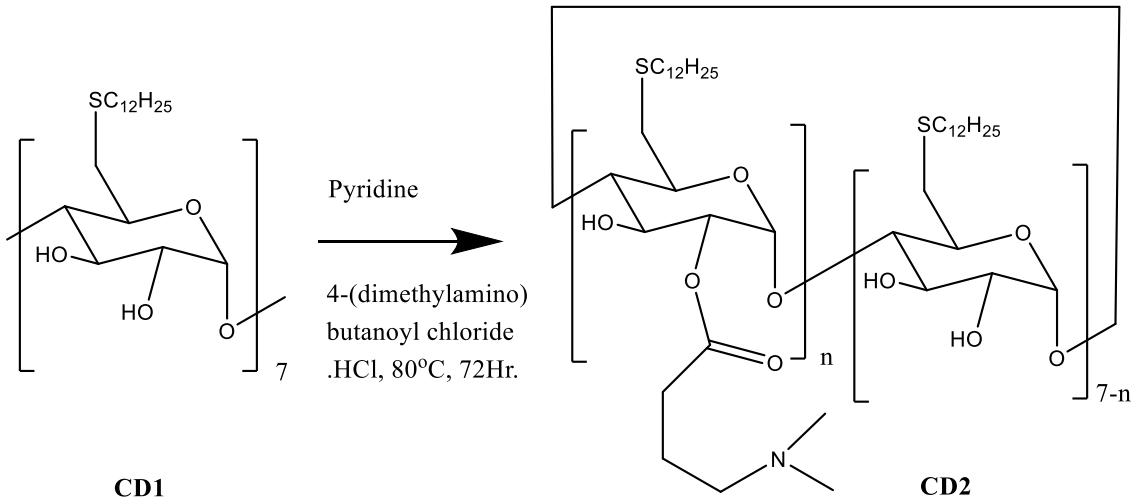

Scheme 1*. *Synthesis of the cationic amphiphilic cyclodextrin (CD2) used as the nanocarrier for siRNA delivery*. *CD1* *(0.121g, 0.05mmol) was dissolved in 6ml dry pyridine under a nitrogen atmosphere. 4-(dimethylamino)butanoyl chloride hydrochloride (106mg, 0.57mmol 1.6 equiv relative to C2-OH) was then added at room temperature. The mixture was stirred for 72 h at 80°C. After cooling, the pyridine was removed in vacuo and the residue was diluted with 25ml $KHSO_4$ (1M). The precipitated material was filtered by gravity, washed with water and dried in vacuo.

The successful synthesis was confirmed by Fourier-Transform infrared spectroscopy (FTIR), nuclear magnetic resonance (NMR) and high-resolution mass spectrometry (HRMS), as follow:

FT-IR (cm^{-1}, KBr disc): 3347, 2956, 2923, 2852, 1734, 1467, 1194, 1154, 1040.

^{1}H NMR (600MHz, $CDCl_3$) δ 4.5-5.1 (broad, 4H), 3.84 (s, 1H), 3.40 (s, 1H), 3.14 (s, 1H), 2.95 (s, 1H), 2.84 (s, 3H), 2.52 (s, 2H), 2.00 (s, 1H), 1.50 (s, 2H), 1.29 (s, 2H), 1.19 (s, 18H), 0.78 (t, j=7.2Hz, 3H).

^{13}C NMR (151MHz, $CDCl_3$) δ 175.64, 172.71, 102.14, 99.36, 83.97, 73.34, 71.81, 71.25, 70.56, 69.76, 56.93, 43.33, 33.63, 31.99, 30.96, 29.86, 29.79, 29.71, 29.67, 29.60, 29.46, 22,73, 14.15.

HRMS: Calculated for CD2 n = 4, $C_{150}H_{287}N_4O_{32}S_7$ $[M+5H]^+$: 2880.9000g/mol. Observed: 2880.8894g/mol. Discrepancy: 3.7ppm. Calculated for $C_{150}H_{285}N_4O_{32}S_7$ $[M+3H]^+$: 2878.8840g/mol. Observed: 2878.8837g/mol. Discrepancy: 0.1ppm.

Calculated for CD2 n = 5, $C_{156}H_{298}N_5O_{33}S_7$ $[M+5H]^+$: 2993.984g/mol. Observed: 2993.96973g/mol. Discrepancy: 4.8 ppm

The adamantyl-PEG_{500}-RVG (herein referred to as Adm.PEG.RVG) was used to form the RVG targeted NPs by formation of an inclusion complex with the CD [20,21].The Adm.PEG.RVG construct was dissolved in distilled water (1 mg/mL) and added to the CDs:siRNA at a mass ratio 10:1:5 (CDs:siRNA:Adm.PEG.RVG) and incubated at 25°C and 450 rpm for 30 min in a thermomixer.

For the permeability studies, aqueous solutions of FAM-labeled siRNA alone or loaded into the CDs:siRNA:Adm.PEG.RVG NPs were prepared as above and concentrated by ultrafiltration (typically 2-fold) using centrifugal concentrators Vivaspin 500 (Sartorius, Germany). The filtration units (MW cut-off: 3 kDa) were filled with 500 uL of CDs:siRNA and then centrifuged for 15 min at 15000 rpm and 4°C.

2.3 Physicochemical characterization

2.3.1 Particle size, polydispersity, surface charge, and morphology

The Z-average hydrodynamic diameter, polydispersity index (PDI), and zeta potential were measured by dynamic light scattering (DLS) using a Zetasizer NanoZS® instrument (Malvern Instruments, Worcestershire, UK).

The morphology was verified by transmission electron microscopy (TEM). The samples were deposited to a 400-mesh carbon film copper grid and stained with 2% (w/v) uranyl acetate. After drying, the grids were examined under a JEOL Transmission Electron Microscope (TEM) JEM 2000FXII (Jeol Ltd., Tokyo, Japan), operated at 160 kV.

2.3.2 Determination of the pK_a value. The 2- (p-toluidino)-6-naphthalene sulfonic acid (TNS) assay was used to determine the apparent pK_a of the cationic CD [22,23]. Measurements were performed in triplicates on black 96-well plates, with each well containing 90 µL of buffers from pH 5.5 to 9.5 in increments of 0.5 pH units (20 mM citrate buffer (pH 5.50–6.50), 20 mM sodium phosphate buffer (pH 7.00–8.00), or 20 mM Tris-HCl buffer (pH 8.50–9.50), 10 µL of the sample, and 2µL of TNS in DMSO (final concentration of 6 µM). Fluorescence was measured on a Wallac 1420 Victor 2 plate reader (Perkin Elmer, Massachusetts, USA) at 340 nm excitation and 460 nm emission wavelength. The pK_a was determined to be the pH value with 50% of maximal fluorescent intensity calculated using a curve-fit analysis.

2.3.3 Circular Dichroism Spectroscopy

Circular dichroism analysis (Chirascan™-Plus Spectrometer; Applied Photophysics, Surrey, UK) was used to examine the secondary structure of RVG in the

Adm.RVG.PEG construct. Spectra were recorded with three repeats in the far-ultraviolet region (190-260 nm) with a bandwidth of 1.0 nm, a step size of 0.5 nm, and an integration time of 30 s.

2.3.4 Gel retardation assay

The binding and complexation of siRNA were confirmed using agarose gel electrophoresis. Briefly, 26 μL total sample (32 ng/well siRNA) volume was load into 1% w/v agarose gel comprising SafeView Nucleic Acid Stain (2 μg/ml, NBS Biological Cambridgeshire, UK). Gel electrophoresis was done in 1X Tris-borate-EDTA (TBE) buffer for 60 min at 90 V. The visualization was made with a ChemiLITE Chemiluminescence imaging system (Cleaver Scientific, Warwickshire, UK).

The mass ratio was selected based on the results of a pilot study in which the NPs were incubated with siRNA (375 nM) at various mass ratios. At mass ratios lower than 10:1, free/unbound siRNA was detected on the agarose gel.

2.4 Cells

The human cerebral microvascular endothelial cell line (hCMEC/D3) at passage number 24 was purchased from Cedarlane Laboratories (Canada). This cell line has been well characterized as a model of human BBB for drug transport studies [24,25] The hCMEC/D3 cells were seeded onto rat collagen I-coated T75 flasks (CELLCOAT®, Greiner Bio-One) and cultured in Endothelial Growth Medium (EBM-2, #CC-3156) supplemented with SingleQuots™ Bullet-Kit (#CC-4176; 0.5 ng/ml VEGF, 5 ng/ml EGF, 10 ng/ml bFGF, 20 ng/ml long R3-IGF-1, 22.5 μg/ml heparin, 1 μg/ml ascorbic acid, 0.2 μg/ml hydrocortisone, gentamicin (1/1000 dilution) and 2% fetal bovine serum (FBS)), both from Lonza. The growth medium was changed every 2-3 days

until the cells reached approximately 80% confluency. Cell passage was performed by trypsinization using 0.05% Trypsin-EDTA solution. Cells were maintained in a humidified 5% CO_2 incubator at 37 °C. To ensure the maintenance of BBB properties the hCMEC/D3 were used at passage 24 to 34 [24].

Immortalized striatal rat embryonic neurons expressing a high level of human huntingtin fragment (1-548) with 120 glutamines or CAG repeats (ST14A/Q120 High; Coriell, #CH00067) were cultured in DMEM with 4.5g/L glucose, L-glutamine, and sodium pyruvate with 10% FBS and 1% penicillin/streptomycin, herein referred as complete medium. The cell culture medium was changed every 2–3 days. Cells were maintained at 33 °C, with a 5% CO_2 atmosphere.

2.5 Cell viability

hCMEC/D3 cells were seeded at a density of 3 x 10^4 cells/cm^2 on rat tail collagen I (100 µg/ml) and fibronectin (50 µg/ml) coated 24-well inserts (Greiner ThinCert™, 0.4 µm pore size, 0.33 cm^2 growth surface area, transparent). The cells were grown for 8 days up to confluence. To establish a non-toxic concentration for the permeability studies, aqueous solutions of NPs were successively diluted in Hank's Balanced Salt Solution (HBSS) and added to the hCMEC/D3 cells. ST14A (1.5×10^5 cells/mL) cells were seeded onto 96-well plates and allowed to attach for 24 h. The cells were treated with the same concentration used for transfection experiments (75 nM siRNA final concentration).

After 48 h of incubation, the medium was removed and replaced with 50 µl of MTT solution (0.5 mg/mL) and left at 37ºC for 4 h. Then, the MTT solution was removed and 100 µL DMSO was added to dissolve the blue formazan crystals. The absorbance was quantified by a plate reader (Wallac 1420 Victor 2, Perkin Elmer, Massachusetts, USA) at 570 nm and the percentage of viable cells was normalized to control (untreated cells).

2.6 Permeability studies

hCMEC/D3 cells were grown for 8 days up to confluence in coated 24-well inserts. The integrity of hCMEC/D3 monolayer on the inserts was examined by measuring the transendothelial electrical resistance (TEER) using an EVOM2 instrument (World precision Instruments, Florida, USA). Additionally, the apparent permeability coefficient (*P*app) of FITC Dextran 4 kDa (FD4) and immunohistochemical staining of a tight junction-associated protein, ZO-1, were conducted to examine any structural changes in the monolayer.

To measure paracellular permeability, the medium was gently removed and cells were washed twice with HBSS buffer. FD4 (0.4 mg/mL in HBSS) was added to the upper compartment (total volume of 150 µl) and then incubated at 37^{o}C on an orbital shaker with moderate speed. At predetermined times (30, 60, 120, 180, and 240 min) 50 µL sample aliquots were withdrawn from the lower compartment (total volume of 600 µL) and transferred to a black 96-well plate. The quantity of FD4 that diffused through the monolayer into the lower compartment at each time point was determined using a plate reader (Wallac 1420 Victor 2, Perkin Elmer). The permeability coefficients were calculated as previously described [26].

Prior to the CD NP permeability studies, aqueous solutions of concentrated NPs were diluted by 5-fold in HBSS and then the analysis was performed as described above. At the end of the experiment, the inserts were fixed with 10% (w/v) trichloroacetic acid (TCA) and then the nuclei were stained with DAPI (0.1 mg/mL) to verify the cell monolayer integrity. Additionally, immunohistochemical staining of ZO-1 was performed as described below.

2.7. Cellular uptake

ST14A cells (1.5×10^5 cells/mL) were seeded onto coverslips and 24-well plates in 400 µL of DMEM complete medium. After 24 h, 100 µL of CDs containing FAM-labeled siRNA (at a final concentration of 75 nM siRNA) were added to the cells and incubated at 37°C. After 6 h, the coverslips were washed twice with PBS and fixed with 10% TCA for 15 min. After washing, nuclei were stained with DAPI for 5 min. Finally, the intracellular fluorescence distribution was visualized under an Olympus IX73 microscope (Olympus Inc., Tokyo, Japan). Cellular uptake was detected by BD LSR II Flow cytometry (minimum 40,000 events) at the wavelength of 488 nm.

2.8 Gene expression analysis

To detect the relative expression level of *HTT* mRNA, ST14A cells were analyzed by quantitative reverse transcription PCR (RT-qPCR) after monoculture and co-culture with hCMEC/D3 cells. Co-culture models were prepared by seeding hCMEC/D3 cells (3×10^4 cells/mL) in 24-well inserts, 7 days prior to ST14A cell seeding. Subsequently, ST14A cells (1.5×10^5 cells per well) were seeded on the bottom of the 24-well plates and cultured for one day before transfection. Free siRNA (75 nM) alone, or CD:siRNA or co-formulated with RVG, was added to the cells in complete DMEM medium. After 48 h, total RNA was extracted from the cells using GenElute™ kit according to the supplier's instructions (Sigma Aldrich). A high-capacity cDNA reverse transcriptase kit (Applied Biosystems, CA, USA) was used for complementary DNA (cDNA) synthesis.

Experiments were carried out using the SensiFAST™ SYBR® Lo-Rox kit (Bioline) in a final volume of 10 µl containing: 5 µl of 2X SensiFAST™ SYBR® Lo-Rox Mix, 0.4 µl of primer mix (400 nM final concentration), 4 µl of diluted cDNA and 0.6 µl of nuclease free water. All reactions were carried out using the CFX96 Real-Time PCR Detection System (Bio-Rad) following the steps: 95 °C for 2 minutes, 40 cycles of

amplification (denaturation at 95 °C for 5 seconds, annealing at 60ºC for 10 seconds, and extension at 72 °C for 20 seconds) and final melt curve analysis from 65 °C to 95 °C to exclude unspecific PCR products. Each reaction was run in duplicate. Results were expressed as Ct values after normalization to18S ribosomal RNA as the housekeeping gene. Results were expressed as % HTT gene expression relative to controls (untreated cells).

2.9 Immunofluorescence

Cells were seeded in coverslips and transfected for 48 h. After a further 24 h incubation in fresh medium, the cells were washed twice with D-PBS and fixed with 10% TCA at 4ºC for 15 min. Subsequently, 0.2% Triton X-100 was added and left at room temperature for 20 min. After blocking by 3% BSA for 30 min at room temperature, cells were incubated with the primary antibody diluted in 1% BSA (1:100) overnight at 4 °C. Following incubation, the cells were washed twice with D-PBS and the secondary antibody (1:200) was added at room temperature and incubated (1hr) in the dark. The samples were mounted with ProLong™ Gold anti-fade reagent (ThermoScientific), dried, and imaged using an Olympus IX73 microscope (Olympus Inc., Tokyo, Japan).

2.10 Statistical analysis

The statistical analysis was performed using GraphPad Prism 7.0 (GraphPad, San Diego, CA, USA). Data were expressed as mean ± SEM from at least three independent experiments. One-way analysis of variance (one-way ANOVA), followed by Dunnet or Tukey post hoc tests was used to determine the statistical significance between three or more groups. Student's *t*-test was used for comparisons between two groups. A $p < 0.05$ was considered significant.

3. Results and Discussion

For successful treatment of CNS diseases, restricted access of therapeutic molecules across BBB needs to be overcome. Currently, several brain-targeting ligands have been exploited as a strategy for brain delivery of therapeutics. Endothelial cells have many receptors on their surface to enable the transport of small and large molecules. Via receptor-mediated transcytosis, a receptor can specifically bind to its ligand on the luminal side of the endothelium and trigger internalization into cells [5]. Thus, specific ligands could be functionalized onto the surface of NPs to mediate their transport across the BBB. Kumar et al. demonstrated the important concept that an AChR-binding peptide derivate from RVG conjugated to polyarginine (9R), which enable siRNA binding through electrostatic interactions, can deliver siRNAs to neuronal cells and potentially other therapeutic molecules across the BBB [27]. In this study, to enhance permeability across the BBB and subsequently achieve neuronal-targeting, the RVG peptide was inserted via inclusion complex formation into the amphiphilic CDs for the delivery of siRNA targeting *HTT*.

3.1 Nanoparticle characterization

CDs are highly versatile oligosaccharides that can be easily modified to change their physicochemical properties due to the presence of numerous hydroxyl groups on the ring structure (O'Mahony et al 2013). In order to reduce the cationic nature of the CDs used in our previous studies, the pK_a of the primary amine group was altered by incorporating a tertiary amine (Scheme 1), resulting in a decrease in the pK_a from approximately 11 to 6.57 (Figure 1A). In the case of cationic lipids, a pK_a in the range of 6.2-6.5 is considered optimal for successful nucleic acid delivery and efficient gene silencing [28]. The successful synthesis was confirmed by FTIR, NMR and HRMS. The FTIR spectrum showed characteristics bands corresponding to the SC12 chain and CD

backbone (Figure 1B). A strong absorption peak at 3347 cm^{-1} (O-H stretching vibration) and peaks at 2852 cm^{-1} (C–H assymetric/symmetric stretching), 1154 (C-O vibration) and 1040 cm^{-1} (C–O stretching) [29,30]. The HRMS analysis indicated substitution patterns at C2, with sample signals definitive for n = 4 and n = 5 substitution.

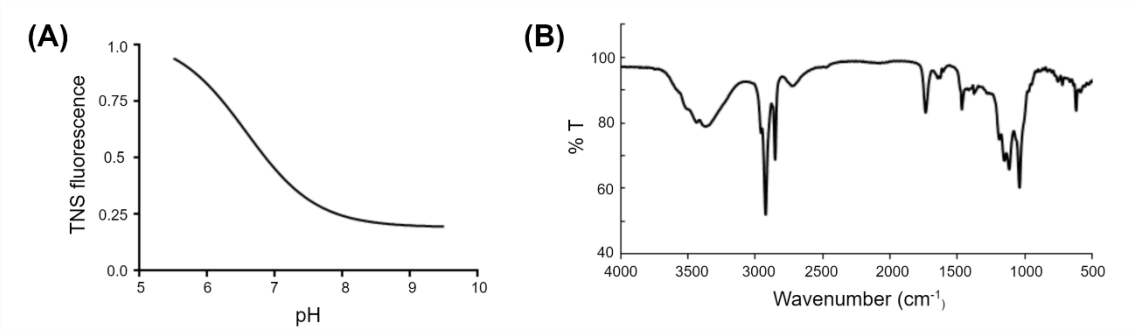

Figure 1. ***Physicochemical characterization***. *(A) In situ TNS fluorescence titration for determining the pKa of the CD and (B) FTIR spectra.*

The Z-average diameter of the CDs.siRNA complex was 169 ± 6.20 nm with a PDI 0.38 ± 0.014. Further formulation optimization by the addition of the Adm.PEG.RVG to the CDs:siRNA increased the hydrodynamic diameter to 187 ± 5.71 and improved the PDI to 0.33 ± 0.014. Since size is an important physicochemical property that affects the endocytosis of a molecule by the brain capillary cells, the size distribution is generally controlled to under 200 nm to enhance the potential of efficiently crossing the BBB [31]. The spherical morphology of the CD NPs was confirmed by TEM (Figure 2A).

The surface charge, measured by zeta potential, was similar between targeted and untargeted CDs (15-16 mV), indicating that addition of the RVG peptide did not markedly affect the positive surface charge. Overall, the current CD formulation meets the critical quality attributes for optimum BBB permeability following systemic administration including appropriate particle size (169-187 nm), and a slightly positive charge (15-16 mV) [31].

The gel retardation assay confirmed that the CDs strongly bound the siRNA at a mass ratio of 10:1, no displacement of siRNA was detected with the addition of the Adm.PEG.RVG (Figure 2B). Preliminary optimization studies identified the specific ratios of 10:1 for CDs:siRNA and 10:1:5 for CDs:siRNA:Adm.PEG.RVG, and these were used in the subsequent work.

The presence of intact RVG in the Adm.PEG.RVG construct was confirmed using circular dichroism (Figure 2C). In the far-UV circular dichroism spectra, pure RVG exhibited a broad negative band at ~206 nm, characteristic of proteins with no dominant secondary structure (a random coil) [32]. The Adm.PEG.RVG presented a similar CD spectrum, albeit with a lower signal intensity as expected due to the lower concentration of RVG.

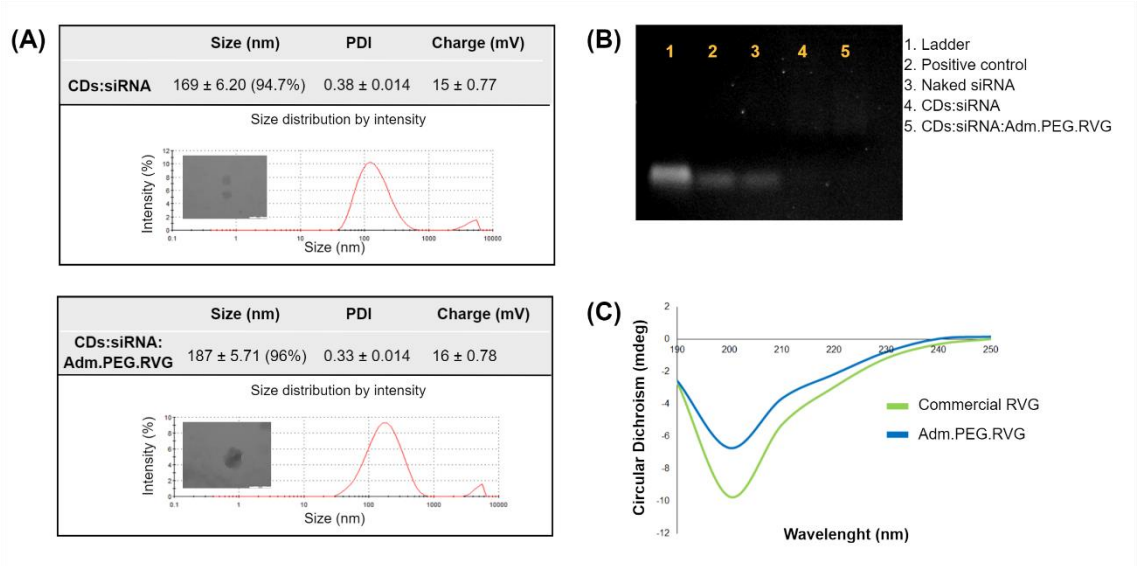

Figure 2. Physicochemical characterization of the cationic amphiphilic cyclodextrin (CD) used as the nanocarrier for siRNA delivery. *(A) Dynamic light scattering measurements of CDs:siRNA (mass ratio 10:1) and CDs:siRNA:Adm.PEG.RVG (mass ratio 10:1:5). Inset: TEM image of nanoparticles; (B) Representative agarose gel electrophoresis illustrating siRNA complexation by CDs; (C) Circular dichroism spectra of commercial RVG and Adm.PEG.RVG in aqueous solution (1 mg/mL); Mean ± S.E.M of 6 independent syntheses.*

3.2 Establishment of an *in vitro* human BBB model

Over the last decade, a large number of *in vitro* BBB models have been developed to mimic the physiological characteristics and simulate the complexities of the BBB including organoids, spheroids, BBB-on-chip models, induced pluripotent stem cells (iPSC)-in microfluidic platforms, and other innovative technologies [33,34]. However, since cost and test capacity are important factor in industrial drug screening, models based on immortalized cell lines, especially human hCMEC/D3, are still among the most used to predict permeability of CNS drug candidates [24,25]. In this study, a widely adopted *in vitro* human BBB model based on hCMEC/D3 cells was established and characterised.

The hCMEC/D3 cells were grown on permeable membrane inserts for 8 days (Figure 3A) and the integrity of the paracellular junctions was measured by evaluating the small 4 kDa FITC-dextran (FD4) molecule and performing TEER measurements. In the absence of cells (membrane alone), free diffusion of FD4 occurred with a significantly higher permeability of *P*app of 7.62 ± 0.27 x 10^{-6} cm/s compared to a *P*app of 4.88 ± 0.23 x 10^{-6} cm/s in the presence of cells (** p = 0.0015) (Figure 3B). These values correlate well with those previously reported for a confluent monolayer [35,36].

As shown in Figure 3C, TEER values were approximately 25 Ω cm^2 after 6 days and reached a plateau at approximately 20 Ω cm^2 by day 7. Although far from TEER values observed in other cell based BBB models (>100 Ω cm^2) [37], the TEER values are in accordance to those reported in other studies for this cell line [38–40].

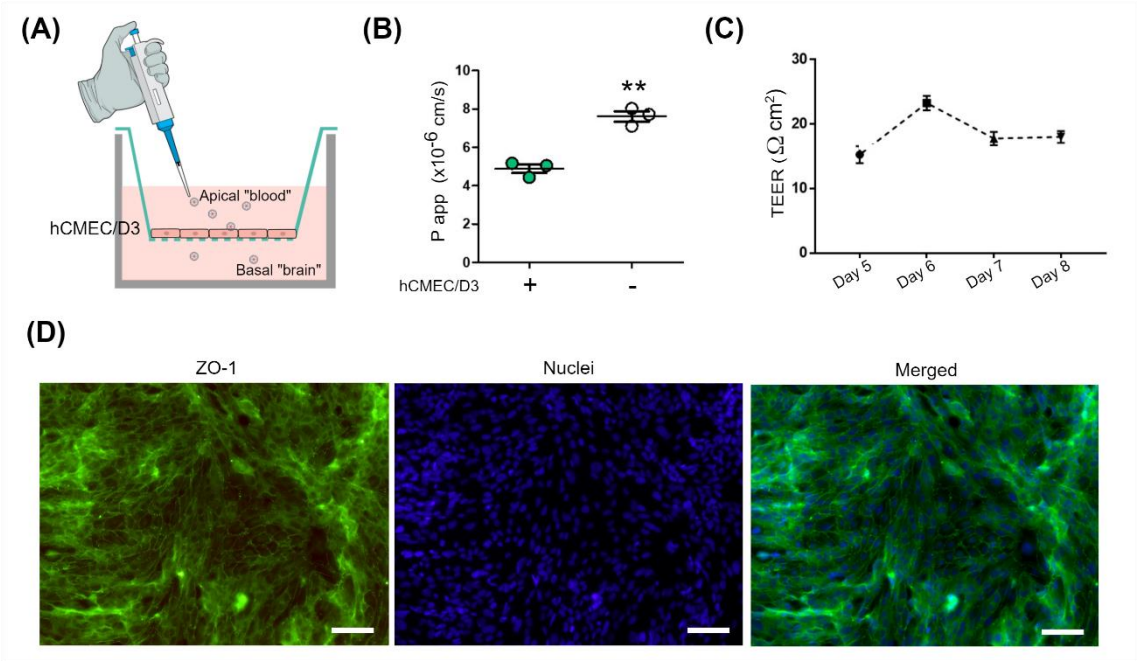

Figure 3. Functional characterization of the in vitro blood-brain barrier (BBB) model*. (A) Schematic illustration of in vitro transwell BBB system; (B) Permeability values of 4 kDa FITC-Dextran from apical to basal compartments, in the presence (green circles) and absence (white circles) of hCMEC/D3 cells. Fluorescence was measured in the basal chamber after 4h; (C) Transepithelial/endothelial electrical resistance (TEER) measurements; (D) Representative tight junction ZO-1 (green) and nucleus (blue) immunofluorescence staining of hCMEC/D3 cells, scale bar = 50 µm; Values are reported as the mean ± S.E.M and correspond to three independent experiments. T-test ** $p \leq 0.01$.*

The hCMEC/D3 cell line constitutively expresses many endothelial markers including the junctional proteins PECAM-1 and JAM-A, as well as the adherens and tight junction proteins VE-cadherin, claudin-5, β- and γ-catenins and ZO-1 [41]. Since tight junctions are crucial in controlling paracellular transport, including dextrans, the expression of the tight junction protein ZO-1 was assessed. ZO-1 showed a typical localization at the cell-cell boundaries (Figure 3D), which confirms the formation of a confluent and uniformly-stained cell monolayer on the inserts.

3.3 Evaluation of the cellular viability and fluorescent tracer permeability

Prior to clinical translation, the toxicity of NPs is a significant factor to be considered. To determine a safe treatment concentration of NPs for further experiments,

the response of hCMEC/D3 to incubation with free siRNA, CDs:siRNA and CDs:siRNA:Adm.PEG.RVG in different dilutions of HBSS was monitored after 48 h. A dose-dependent toxic effect was observed, with cell viability above 80% when diluted in 20% (v/v) HBSS (Figure 4). In accordance with the International Organization for Standardization (ISO) 10993-5, percentages of cell viability above 80% are considered non-toxic [42]. Although the slight differences in viability (4:1 in HBSS) relative to the control (untreated cells) were statistically significant, DAPI nuclear staining was similar between both groups, implying that CDs:siRNA and CDs:siRNA:Adm.PEG.RVG (4:1 in HBSS) exhibited good biocompatibility.

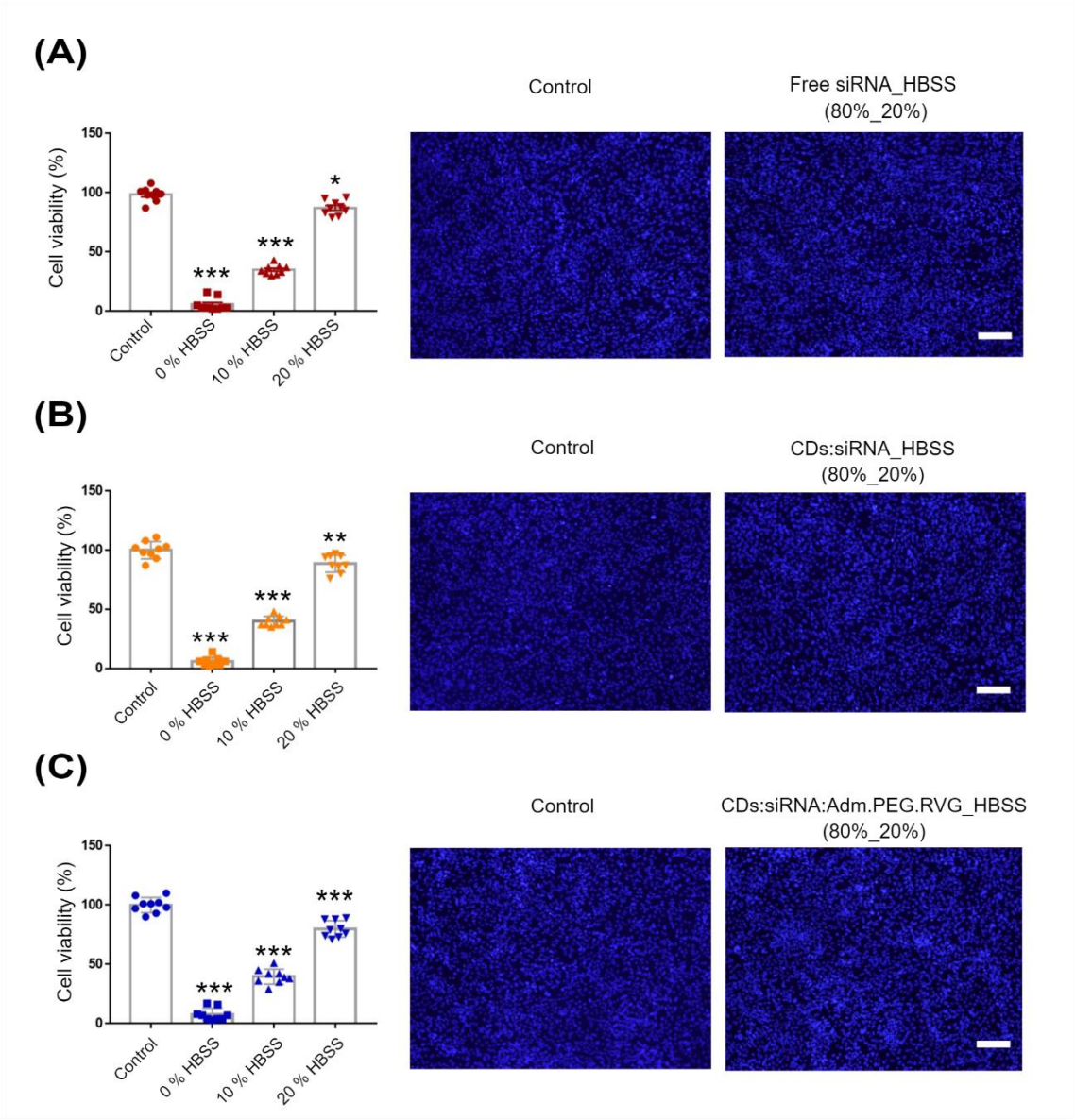

Figure 4. Cytotoxicity profile of cyclodextrins (CDs) in hCMEC/D3 cells. *Viability of hCMEC/D3 cells treated with (A) Free siRNA, (B) CDs:siRNA and (C) CDs:siRNA:Adm.PEG.RVG diluted in HBSS (0%, 10% and 20%, v/v), 75 nM siRNA final concentration. Representative microscopy images of hCMEC/D3 monolayer with DAPI fluorescence (blue) at 48 h post-treatment, scale bars = 100 µM. Living cells were determined using an MTT assay and expressed as a % of the control. Mean ± S.E.M of 3 technical replicates performed in triplicate. One-way ANOVA followed by Dunnet's post hoc test. * $p \leq 0.05$, ** $p \leq 0.01$, *** $p \leq 0.001$.*

To determine the permeability of tracers across the monolayer, FAM-labeled siRNA was loaded into targeted and untargeted CD NPs and added to the apical compartment of the BBB model. After 30, 60, 120, and 240 min incubation time, aliquots from the basal compartment were collected, and the amount of siRNA that crossed the monolayer was quantified by measuring the fluorescent intensity. A gradual increase of

siRNA content in the basal compartment over time demonstrated that the siRNA loaded into target CD NPs progressively permeated the monolayer barrier (Figure 5). Compared to untargeted CDs, siRNA loaded into target CD NPs (CDs:siRNA:Adm.PEG.RVG) showed higher penetration across the cell layer after 4 h. However, the lack of statistically significant differences suggested that not only the targeting moiety but also the CD delivery system itself, plays a significant role in enhancing the membrane permeability of the NPs. The permeability enhancing effects of CDs are strongly dependent on the nature and/or chemical modification of the CD [43]. Typically, CDs are unable to overcome the BBB, however, modified CDs have been proven to successfully transport molecules across the BBB. β-CDs cross-linked with poly(β-amino ester) for doxorubicin transport successfully cross human brain endothelial cell monolayers without affecting the barrier integrity presumably due to the tertiary amine groups incorporated, which can be positively charged under physiological conditions [44]. Quaternary ammonium chitosan-methyl-β-CDs NPs have also shown successful delivery of the neuropeptide Dalargin across the BBB (bEnd.3 cells BBB model) by the transcellular route [45]. Mostly, transcellular transport occurs *via* passive diffusion while peptides depend on specific transporters to enter the brain.

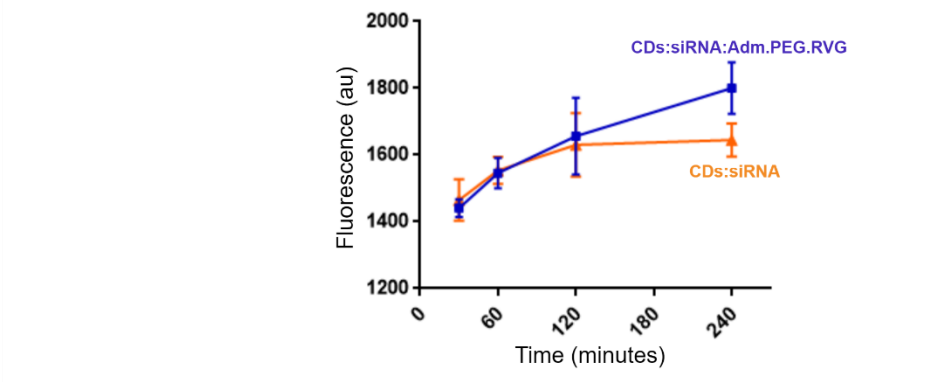

Figure 5. Evaluation of targeted and untargeted CDs NPs permeability. *Penetration of siRNA within CDs:siRNA:Adm.PEG.RVG (blue line) and CDs:siRNA (orange line) NPs across hCMEC/D3 monolayer over 4 h, mimicking BBB transport conditions. Fluorescence (arbitrary units (au)) was measured in the basal compartment at given time points. Data are reported as mean ± S.E.M and correspond to five independent experiments.*

3.4 Effect of RVG targeting on cellular uptake and HTT silencing

Considering that efficient cellular uptake is a premise for achieving gene silencing [46], the ability of the CD-NPs to deliver siRNA into diseased cells was evaluated. For this purpose, the rat striatal embryonic neuronal cell line ST14A that constitutively expresses human mHTT, a widely used cellular model of HD was used [18]. FAM-labeled siRNA alone or FAM-labelled siRNA loaded into CDs co-formulated with and without RVG was incubated with the cells for 6 h. Following transfection, little or no fluorescence was observed following treatment with siRNA alone. In contrast, strong signals were detected for following treatment with CDs:siRNA and CDs:siRNA:Adm.PEG.RVG indicating the ability of the CD-NPs to promote neuronal cell uptake of siRNA. The siRNA fluorescence was observed in the cytoplasm and near the nucleus of most of the neurons in the culture, demonstrating an efficient and uniform uptake (Figure 6A). Several studies have demonstrated that RVG peptide conjugated to nanomaterials can deliver siRNA, miRNA, and DNA across the BBB and promote preferential accumulation of loaded nucleic acids in neuronal cells [17,47–50] via the nAChRs expressed by brain endothelial cells and neuronal cells [17].

The levels of uptake were also determined by flow cytometry. As shown in Figure 6B, while no significant uptake was detected for naked siRNA, enhanced siRNA uptake by ST14A cells was detected for the CD-NPs in the order of CDs:siRNA:Adm.PEG.RVG (61.3 %) > CDs:siRNA (53.3 %) > Free siRNA (4.89%) (Figure 6B), although no statistical differences were observed between targeted and non-targeted NPs. In addition, the complexation of RVG to CDs did not affect cell viability (> 80% cell viability compared to untreated cells), as assessed by MTT assay (Figure S1).

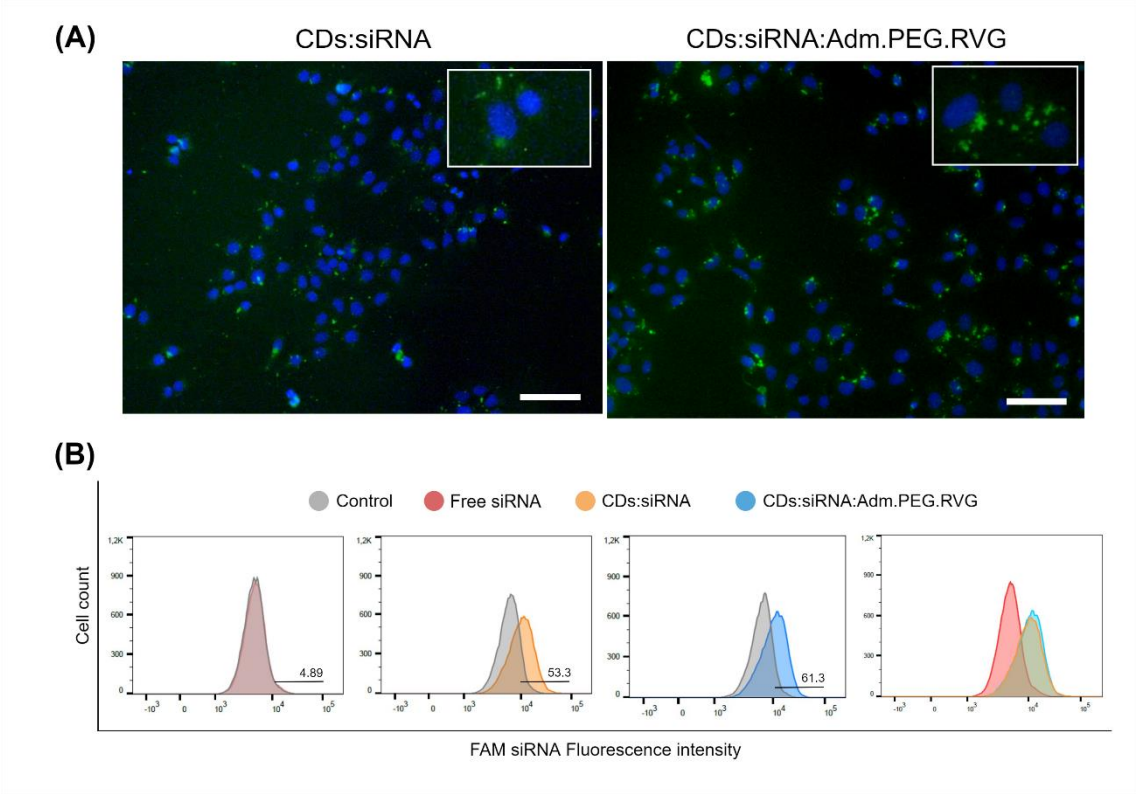

Figure 6. Cyclodextrins (CDs) mediate siRNA delivery in a cellular model of Huntington`s disease*. ST14A cells were treated with siRNA alone or complexed with CDs and the cellular uptake confirmed by (A) fluorescence microscopy and (B) flow cytometry after 6 h of incubation. Images of FAM-labeled siRNA (green) positive cells are shown with the nuclei stained by DAPI (blue). Insets illustrate higher magnification, scale bars = 50 μm.*

After demonstrating that the CD NPs efficiently delivered siRNA into target cells, the ability of the NPs to cross the BBB and induce silencing of *HTT* mRNA, the single gene responsible for the development of Huntington's disease, was evaluated. The model used was established by culturing hCMEC/D3 cells in the apical compartment and ST14A cells in the basal compartment of an insert to simulate the *in vivo* environment where permeability across the BBB followed by diffusion to the target disease cells is required for therapeutic efficacy (Figure 7A). There are, to our knowledge, no reports of a co-culture model using the hCMEC/D3 BBB cell line and the ST14A striatal neuronal cell model of HD.

After 48 h of transfection, both untargeted and targeted CD-NPs mediated *HTT* gene knockdown in ST14A cells. *HTT* mRNA levels were reduced to 65 ± 3.88 % and

54 ± 3.57 % when the cells were transfected with CDs:siRNA and CDs:siRNA:Adm.PEG.RVG, respectively, compared to control ($p < 0.001$) (Figure 7B). Although the RVG-targeted CDs exhibited a higher silencing activity, no statistical difference was observed compared to untargeted CDs ($p = 0.0629$), which is in agreement with cellular uptake results.

The *HTT* mRNA levels after direct incubation of NPs in the ST14A cells alone (monoculture) were also evaluated (Figure S2). *HTT* mRNA levels were similar in the ST14A monoculture compared to the co-culture model: 67 ± 3.57 % *vs.* 65 ± 3.88 %, respectively, for CDs:siRNA and 57 ± 3.14 % *vs.* 54 ± 3.57 %, respectively, for CDs:siRNA:Adm.PEG.RVG. As naked siRNA fails to show significant cellular uptake (Figure 6) and produces no significant gene knockdown (Figure S2), these results imply that the CD-NPs are capable of promoting uptake and gene silencing in the target ST14A cells.

Gene silencing at the protein level was confirmed by immunostaining ST14A cells, from the co-culture model, against HTT antibody (Figure 7C). A wide-spread HTT immunoreactivity was detected throughout the cytoplasm of ST14A untreated cells (control group). HTT immunoreactivity, evaluated by fluorescence intensity, was reduced after exposure to both CDs:siRNA and CDs:siRNA:Adm.PEG.RVG NPs, compared to the control and naked siRNA. As expected, HTT positive cells were much more abundant for CDs:siRNA than CDs:siRNA:Adm.PEG.RVG, in line with RT-qPCR results. No significant downregulation was observed when cells were transfected with naked siRNA.

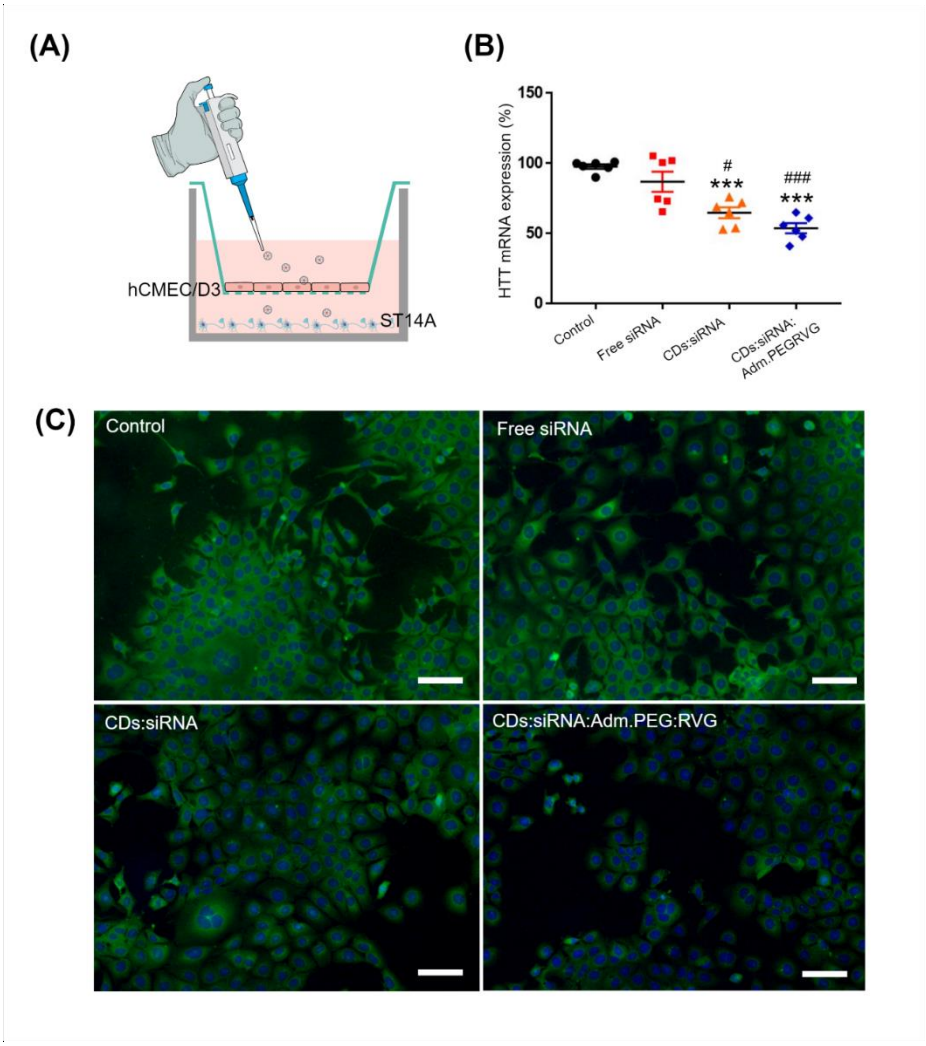

Figure 7. Efficient downregulation of HTT by CD.siRNA NPs in the co-culture model. *(A) Schematic illustration of in vitro co-culture system containing hCMEC/D3 (apical side) and ST14A cells (basal side); (B) mRNA levels of HTT in ST14A cells measured 48 h post-transfection by SYBR Green qPCR and normalized to 18S ribosomal; (C) Representative images of ST14A cells showing expression of Huntingtin (HTT) protein (green) with the nuclei stained by DAPI (blue) 72 h post-transfection, scale bar = 50 μM. n = 6, three independent experiments. Mean ± S.E.M. One-way ANOVA with Tukey multiple comparisons test. ***p < 0.001 compared to control; #p < 0.05 and ###p < 0.001 compared to Free siRNA.*

While the RVG targeted NP resulted in greater gene silencing *versus* the untargeted NPs, the differences were not statistically significant. The relatively small difference between targeted and untargeted CDs can potentially arise from several factors. Firstly, the contribution of the RVG peptide, may be masked by the variability of the physiological cellular environment (*i.e* Fetal bovine serum (FBS)-supplemented culture media). Adsorption of proteins in serum could reduce or block the binding of ligand-modified NPs to their specific receptors decreasing the targeting efficiency [51,52].

PEGylating the surface of the NPs may help to overcome this issue [52]. Secondly, the ligand density and orientation on the surface of the NPs can also influence the ligand-receptor engagement. In general, as the density increases, the fraction of NPs that bind to the receptors/targets on the cell membrane increases until the optimum density is reached, further increases in density have been shown to result in a decrease in receptor binding due possibly to a hindering stearic effect [53]. Further studies to optimize the ligand density may help to improve the target specific uptake and thus enhance the gene silencing efficacy.

Although optimization of the delivery system is still necessary, CD-NPs platforms represents an alternative to overcome the delivery limitations of free chemically modified nucleic acids, which require administration directly into the brain or cerebrospinal fluid. Even the most promising HTT-lowering ASO, was discontinued by Roche following a poor risk-benefit analysis. The investigators reported no overall benefit compared to a placebo, in addition, drug-related increases in brain ventricular volume were detected, including five confirmed cases of hydrocephalus in patients receiving the higher-frequency intrathecal dosing [54]. Therefore, efforts to develop less invasive delivery platforms, including nanoparticles, for chemically modified nucleic acids are highly desirable.

4. Conclusion

The development of an effective gene delivery system remains a challenge for the clinical application of siRNA therapeutics in brain diseases. Taken together the results strongly supported the hypothesis that the siRNA delivered by CD-NPs was released into the cytoplasm of neuronal cells and further mediated partial silencing of the HTT gene regardless of the targeting moieties, although the silencing efficacy of the target NPs was 20% higher than the untargeted formulation. In-depth *in vivo* studies using animal models

of HD are required to elucidate the mechanisms of transport across the BBB and assess the potential of the delivery system to translate into the clinic.

Declaration of Competing Interest

The authors declare that they have no known competing financial interests or personal relationships that could have appeared to influence the work reported in this paper.

Acknowledgments

This publication has emanated from research supported in part by a grant from Science Foundation Ireland (SFI) and the European Regional Development Fund (ERDF) under grant number 13/RC/2073_2. Centre for Research in Medical Devices, CÚRAM.

References

[1] F. Saudou, S. Humbert, The Biology of Huntingtin, Neuron. 89 (2016) 910–926. https://doi.org/10.1016/j.neuron.2016.02.003.

[2] S. Tabrizi, M.D. Flower, C.A. Ross, E.J. Wild, Huntington disease: new insights into molecular pathogenesis and therapeutic opportunities, Nat. Rev. Neurol. 16 (2020) 529–546. https://doi.org/10.1038/s41582-020-0389-4.

[3] K.M. Shannon, Recent Advances in the Treatment of Huntington's Disease : Targeting DNA and RNA, CNS Drugs. 34 (2020) 219–228. https://doi.org/10.1007/s40263-019-00695-3.

[4] S. Tabrizi, R. Ghosh, B.R. Leavitt, Huntingtin Lowering Strategies for Disease Modification in Huntington's Disease, Neuron. 101 (2019) 801–819. https://doi.org/10.1016/j.neuron.2019.01.039.

[5] M. Mendonça, A. Kont, M. Aburto, J. Cryan, C. O'Driscoll, Advances in the design of (Nano)formulations for delivery of antisense oligonucleotides and Ssmall interfering RNA: Focus on the central nervous system, Mol. Pharm. 18 (2021) 1491–1506. https://doi.org/10.1021/acs.molpharmaceut.0c01238.

[6] W.F. Kaemmerer, R.C. Grondin, The effects of huntingtin-lowering : what do we know so far ?, Degener. Neurol. Neuromuscul. Dis. 9 (2019) 3–17.

[7] G.C. Terstappen, A.H. Meyer, R.D. Bell, W. Zhang, Strategies for delivering therapeutics across the blood–brain barrier, Nat. Rev. Drug Discov. (2021). https://doi.org/10.1038/s41573-021-00139-y.

[8] C. Xu, B. Yu, Y. Qi, N. Zhao, F. Xu, Versatile Types of Cyclodextrin-Based Nucleic Acid Delivery Systems, Adv. Healthc. Mater. 2001183 (2021) 1–19. https://doi.org/10.1002/adhm.202001183.

[9] H. Mousazadeh, Y. Pilehvar-soltanahmadi, M. Dadashpour, Cyclodextrin based natural nanostructured carbohydrate polymers as effective non-viral siRNA delivery systems for cancer gene therapy, J. Control. Release. 330 (2021) 1046–1070.

https://doi.org/10.1016/j.jconrel.2020.11.011.

[10] S.S. Jambhekar, P. Breen, Cyclodextrins in pharmaceutical formulations I : structure and physicochemical properties , formation of complexes , and types of complex, Drug Discov. Today. 21 (2016) 356–362. https://doi.org/10.1016/j.drudis.2015.11.017.

[11] S. Jacob, A.B. Nair, Cyclodextrin complexes : Perspective from drug delivery and formulation, Drug Dev. Res. (2018) 201–217. https://doi.org/10.1002/ddr.21452.

[12] J.C. Evans, M. Malhotra, K. Sweeney, R. Darcy, C.C. Nelson, B.G. Hollier, C.M. O'Driscoll, Folate-targeted amphiphilic cyclodextrin nanoparticles incorporating a fusogenic peptide deliver therapeutic siRNA and inhibit the invasive capacity of 3D prostate cancer tumours, Int. J. Pharm. 532 (2017) 511–518. https://doi.org/10.1016/j.ijpharm.2017.09.013.

[13] J.C. Evans, M. Malhotra, K.A. Fitzgerald, J. Guo, M.F. Cronin, C.M. Curtin, F.J.O. Brien, R. Darcy, C.M. O'Driscoll, Formulation and Evaluation of Anisamide-Targeted Amphiphilic Cyclodextrin Nanoparticles To Promote Therapeutic Gene Silencing in a 3D Prostate Cancer Bone Metastases Model, Mol. Pharm. 14 (2017) 42–52. https://doi.org/10.1021/acs.molpharmaceut.6b00646.

[14] J. Guo, E.G. Russell, R. Darcy, T.G. Cotter, S.L. Mckenna, M.R. Cahill, C.M. O'Driscoll, Antibody-Targeted Cyclodextrin-Based Nanoparticles for siRNA Delivery in the Treatment of Acute Myeloid Leukemia: Physicochemical Characteristics, in Vitro Mechanistic Studies, and ex Vivo Patient Derived Therapeutic E ffi cacy, Mol. Pharm. 14 (2017) 940–952. https://doi.org/10.1021/acs.molpharmaceut.6b01150.

[15] M. Gooding, M. Malhotra, D.J. Mccarthy, B.M.D.C. Godinho, J.F. Cryan, R. Darcy, C.M. O'Driscoll, Synthesis and characterization of rabies virus glycoprotein-tagged amphiphilic cyclodextrins for siRNA delivery in human glioblastoma cells : In vitro analysis, Eur. J. Pharm. Sci. 71 (2015) 80–92.

[16] B.M.D.C. Godinho, J.R. Ogier, R. Darcy, C.M.O. Driscoll, J.F. Cryan, Self-assembling Modified β - Cyclodextrin Nanoparticles as Neuronal siRNA Delivery Vectors: Focus on Huntington's Disease, Mol. Pharm. 10 (2013) 640–649. https://doi.org/doi: 10.1021/mp3003946.

[17] Q. Wang, S. Cheng, F. Qin, A. Fu, C. Fu, Application progress of RVG peptides to facilitate the delivery of therapeutic agents into the central nervous system, RSC Adv. 11 (2021) 8505–8515. https://doi.org/10.1039/d1ra00550b.

[18] G. Chaves, J. Stanley, N. Pourmand, Mutant Huntingtin Affects Diabetes and Alzheimer's Markers in Human and Cell Models of Huntington's Disease, Cells. 8 (2019) 962. https://doi.org/10.3390/cells8090962.

[19] A.M. O'Mahony, J. Ogier, S. Desgranges, J.F. Cryan, R. Darcy, C.M. O'Driscoll, A click chemistry route to 2-functionalised PEGylated and cationic β-cyclodextrins: co-formulation opportunities for siRNA delivery, Org. Biomol. Chem. 10 (2012) 4954. https://doi.org/10.1039/c2ob25490e.

[20] K.A. Fitzgerald, M. Malhotra, M. Gooding, F. Sallas, J.C. Evans, R. Darcy, C.M. O'Driscoll, A novel, anisamide-targeted cyclodextrin nanoformulation for siRNA delivery to prostate cancer cells expressing the sigma-1 receptor, Int. J. Pharm. 499 (2016) 131–145. https://doi.org/10.1016/j.ijpharm.2015.12.055.

[21] M. Malhotra, M. Gooding, J.C. Evans, D. O'Driscoll, R. Darcy, O'Driscol, Cyclodextrin-siRNA conjugates as versatile gene silencing agents, Eur. J. Pharm. Sci. 114 (2018) 30–37. https://doi.org/10.1016/j.ejps.2017.11.024.

[22] J. Zhang, H. Fan, D.A. Levorse, L.S. Crocker, Ionization behavior of amino lipids for siRNA delivery: Determination of ionization constants, SAR, and the impact of lipid p K a on cationic lipid-biomembrane interactions, Langmuir. 27 (2011) 1907–1914. https://doi.org/10.1021/la104590k.

[23] L. Uebbing, A. Ziller, C. Siewert, M.A. Schroer, C.E. Blanchet, D.I. Svergun, S. Ramishetti, D. Peer, U. Sahin, H. Haas, P. Langguth, Investigation of pH-Responsiveness inside Lipid Nanoparticles for Parenteral mRNA Application Using Small-Angle X-ray Scattering, Langmuir. 36 (2020) 13331–13341. https://doi.org/10.1021/acs.langmuir.0c02446.

[24] B. Weksler, I.A. Romero, P. Couraud, The hCMEC/D3 cell line as a model of the human blood brain barrier, Fluids Barriers CNS. 10 (2013) 16. https://doi.org/10.1186/2045-8118-10-16.

[25] B. Sánchez-Dengra, I. González-Álvarez, F. Sousa, M. Bermejo, M. González-Álvarez, B. Sarmento, In vitro model for predicting the access and distribution of drugs in the brain using hCMEC/D3 cells, Eur. J. Pharm. Biopharm. (2021). https://doi.org/10.1016/j.ejpb.2021.04.002.

[26] C. Guccione, M. Oufir, V. Piazzini, D. Elisabeth, E. Andrea, V. Zabela, M. Teresa, M. Camilla, M. Smiesko, M. Hamburger, A. Rita, European Journal of Pharmaceutics and Biopharmaceutics Andrographolide-loaded nanoparticles for brain delivery : Formulation , characterisation and in vitro permeability using hCMEC / D3 cell line, Eur. J. Pharm. Biopharm. 119 (2017) 253–263. https://doi.org/10.1016/j.ejpb.2017.06.018.

[27] P. Kumar, H. Wu, J.L. Mcbride, K. Jung, M.H. Kim, B.L. Davidson, S. Kyung, P. Shankar, N. Manjunath, Transvascular delivery of small interfering RNA to the central nervous system, Nature. 448 (2007) 39–45. https://doi.org/10.1038/nature05901.

[28] P.R. Cullis, M.J. Hope, Lipid Nanoparticle Systems for Enabling Gene Therapies, Mol. Ther. 25 (2017) 1467–1475. https://doi.org/10.1016/j.ymthe.2017.03.013.

[29] C. Yuan, B. Liu, H. Liu, Characterization of hydroxypropyl-β-cyclodextrins with different substitution patterns via FTIR, GC-MS, and TG-DTA, Carbohydr. Polym. 118 (2015) 36–40. https://doi.org/10.1016/j.carbpol.2014.10.070.

[30] H. Rachmawati, C.A. Edityaningrum, R. Mauludin, Molecular inclusion complex of curcumin-β-cyclodextrin nanoparticle to enhance Curcumin skin permeability from hydrophilic matrix gel, AAPS PharmSciTech. 14 (2013) 1303–1312. https://doi.org/10.1208/s12249-013-0023-5.

[31] V. Ceña, P. Játiva, Nanoparticle crossing of blood-brain barrier: A road to new therapeutic approaches to central nervous system diseases, Nanomedicine. 13 (2018) 1513–1516. https://doi.org/10.2217/nnm-2018-0139.

[32] D.M. Rogers, S.B. Jasim, N.T. Dyer, M. Re, J.D. Hirst, Electronic Circular Dichroism Spectroscopy of Proteins, Chem. 5 (2019) 2751–2774. https://doi.org/10.1016/j.chempr.2019.07.008.

[33] D.J. Mc Carthy, M. Malhotra, A.M. O'Mahony, J.F. Cryan, C.M. O'Driscoll, Nanoparticles and the blood-brain barrier: Advancing from in-vitro models towards therapeutic significance, Pharm. Res. 32 (2015) 1161–1185. https://doi.org/10.1007/s11095-014-1545-6.

[34] A. Bhalerao, F. Sivandzade, S.R. Archie, E.A. Chowdhury, B. Noorani, L. Cucullo, In vitro modeling of the neurovascular unit: Advances in the field, Fluids Barriers CNS. 17 (2020) 1–20. https://doi.org/10.1186/s12987-020-00183-7.

[35] P.J. Gaillard, A.G. De Boer, Relationship between permeability status of the blood-brain barrier and in vitro permeability coefficient of a drug, Eur. J. Pharm. Sci. 12 (2000) 95–102. https://doi.org/10.1016/S0928-0987(00)00152-4.

[36] E. De Jong, D.S. Williams, L.K.E.A. Abdelmohsen, J.C.M. Van Hest, I.S. Zuhorn, A filter-free blood-brain barrier model to quantitatively study transendothelial delivery of nanoparticles by fluorescence spectroscopy, J. Control. Release. 289 (2018) 14–22. https://doi.org/10.1016/j.jconrel.2018.09.015.

[37] B. Srinivasan, A.R. Kolli, M.B. Esch, H.E. Abaci, M.L. Shuler, J.J. Hickman, TEER measuments in cells, 2016. https://doi.org/10.1177/2211068214561025.TEER.

[38] M. Ribecco-Lutkiewicz, C. Sodja, J. Haukenfrers, A.S. Haqqani, D. Ly, P. Zachar, E. Baumann, M. Ball, J. Huang, M. Rukhlova, M. Martina, Q. Liu, D. Stanimirovic, A. Jezierski, M. Bani-Yaghoub, A novel human induced pluripotent stem cell blood-brain barrier model: Applicability to study antibody-triggered receptor-mediated transcytosis, Sci. Rep. 8 (2018) 1–17. https://doi.org/10.1038/s41598-018-19522-8.

[39] H.C. Helms, N.J. Abbott, M. Burek, R. Cecchelli, P. Couraud, M.A. Deli, H.J. Galla, I.A. Romero, E. V Shusta, M.J. Stebbins, E. Vandenhaute, B. Weksler, B. Brodin, In vitro models of the blood – brain barrier : An overview of commonly used brain endothelial cell culture models and guidelines for their use, (2016). https://doi.org/10.1177/0271678X16630991.

[40] M.J. Gomes, P.J. Kennedy, S. Martins, B. Sarmento, Delivery of siRNA silencing P-gp in peptide-functionalized nanoparticles causes efflux modulation at the blood-brain barrier, Nanomedicine. 12 (2017) 1385–1399. https://doi.org/10.2217/nnm-2017-0023.

[41] B.B. Weksler, E.A. Subileau, N. Perrière, P. Charneau, K. Holloway, M. Leveque, H. Tricoire-Leignel, A. Nicotra, S. Bourdoulous, P. Turowski, D.K. Male, F. Roux, J. Greenwood, I.A. Romero, P.O. Couraud, Blood-brain barrier-specific properties of a human adult brain endothelial cell line, FASEB J. 19 (2005) 1872–1874. https://doi.org/10.1096/fj.04-3458fje.

[42] I. 10993-5:2009, Biological Evaluation of Medical Devices. Part 5: Tests for In Vitro Cytotoxicity., Int. Organ. Stand. (2009).

[43] V. Monnaert, S. Tilloy, H. Bricout, L. Fenart, R. Cecchelli, E. Monflier, Behavior of a-, b- , and y-Cyclodextrins and Their Derivatives on an in Vitro Model of Blood-Brain Barrier, J. Pharmacol. Exp. Ther. 310 (2004) 745–751. https://doi.org/10.1124/jpet.104.067512.membrane.

[44] E.S. Gil, L. Wu, L. Xu, T.L. Lowe, β-Cyclodextrin-poly (β -Amino Ester) Nanoparticles for Sustained Drug Delivery across the Blood−Brain Barrier, Biomacromolecules. 13 (2012) 3533−3541. https://doi.org/10.1021/bm3008633.

[45] C. Migone, L. Mattii, M. Giannasi, S. Moscato, A. Cesari, Y. Zambito, A.M. Piras, Nanoparticles based on quaternary ammonium chitosan-methyl-β-cyclodextrin conjugate for the neuropeptide dalargin delivery to the central nervous system: An in vitro study, Pharmaceutics. 13 (2021) 1–15. https://doi.org/10.3390/pharmaceutics13010005.

[46] Y. Xia, J. Tian, X. Chen, Effect of surface properties on liposomal siRNA delivery, Biomaterials. 79 (2016) 56–68. https://doi.org/10.1016/j.biomaterials.2015.11.056.

[47] L. Liu, Y. Li, H. Peng, R. Liu, W. Ji, Z. Shi, Targeted exosome coating gene-chem nanocomplex as "nanoscavenger " for clearing a-synuclein and immune activation of Parkinson's disease, Sci. Adv. 6 (2020) eaba3967. https://doi.org/10.1126/sciadv.aba3967.

[48] S. Rodrigues, S. Arora, T. Kanekiyo, J. Singh, Efficient neuronal targeting and transfection using RVG and transferrin- conjugated liposomes, Brain Res. 1734 (2020) 146738. https://doi.org/10.1016/j.brainres.2020.146738.

[49] M. Conceição, L. Mendonça, C. Nóbrega, C. Gomes, P. Costa, H. Hirai, J.N. Moreira, M.C. Lima, N. Manjunath, L. Pereira de Almeida, Intravenous administration of brain-targeted stable nucleic acid lipid particles alleviates Machado-Joseph disease neurological phenotype, Biomaterials. 82 (2016) 124–137. https://doi.org/10.1016/j.biomaterials.2015.12.021.

[50] C. Fu, Y. Xiang, X. Li, A. Fu, Targeted transport of nanocarriers into brain for theranosis with rabies virus glycoprotein-derived peptide, Mater. Sci. Eng. C. 87 (2018) 155–166. https://doi.org/10.1016/j.msec.2017.12.029.

[51] H. Zhang, T. Wu, W. Yu, S. Ruan, Q. He, H. Gao, Ligand Size and Conformation Affect the Behavior of Nanoparticles Coated with in Vitro and in Vivo Protein Corona, ACS Appl. Mater. Interfaces. 10 (2018) 9094–9103. https://doi.org/10.1021/acsami.7b16096.

[52] W. Xiao, H. Gao, The impact of protein corona on the behavior and targeting capability of nanoparticle-based delivery system, Int. J. Pharm. 552 (2018) 328–339. https://doi.org/10.1016/j.ijpharm.2018.10.011.

[53] A.M. Alkilany, L. Zhu, H. Weller, A. Mews, W.J. Parak, M. Barz, N. Feliu, Ligand density on nanoparticles: A parameter with critical impact on nanomedicine, Adv. Drug Deliv. Rev. 143 (2019) 22–36. https://doi.org/10.1016/j.addr.2019.05.010.

[54] K. Kingwell, Double setback for ASO trials in Huntington disease, Nat. Rev. Drug Discov. 20 (2021) 412–413. https://doi.org/10.1038/d41573-021-00088-6.

Supplementary information

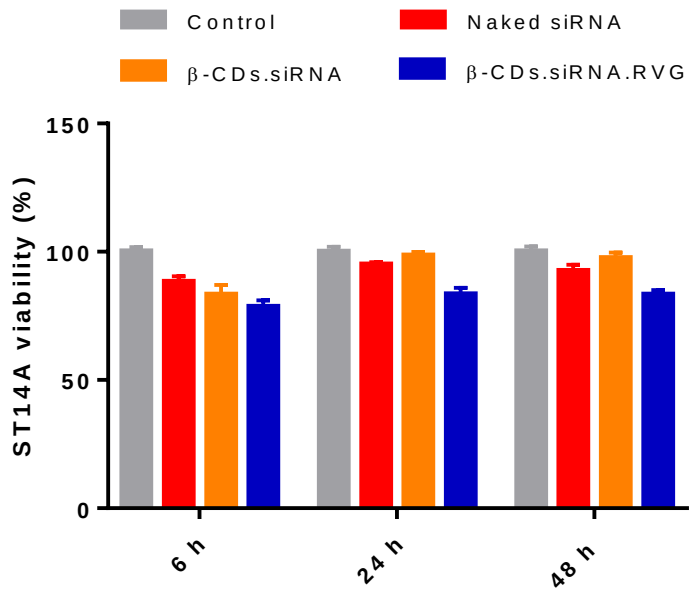

Figure S1. Cell viability of the ST14A cells. *Viability of ST14A cells were determined using an MTT assay and expressed as a percentage of the non-treated cells. Mean ± S.E.M of 3 technical replicates performed in triplicate.* One-way ANOVA followed *by Dunnet's post hoc test.*

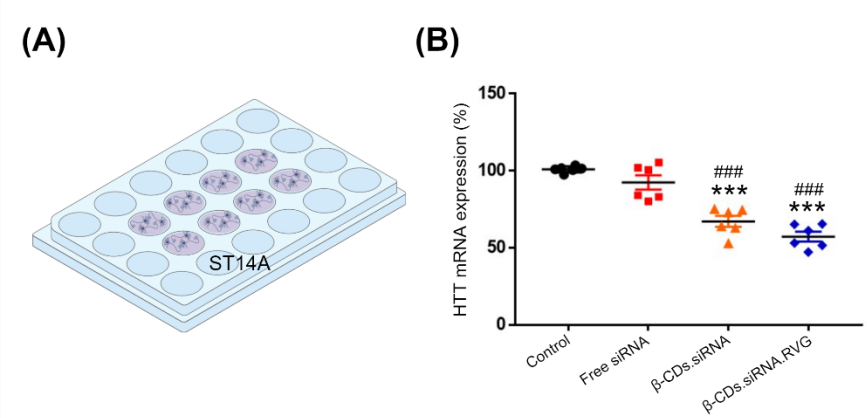

Figure S2. Efficient downregulation of HTT by siRNA. *(A) Schematic illustration of in vitro monoculture system of ST14A cells; (B) mRNA levels of HTT of ST14A cells measured 48 h post-transfection by SYBR Green qPCR and normalized to 18S ribosomal. n = 6, three independent experiments. Mean ± S.E.M. One-way ANOVA with Tukey multiple comparisons test. ***p < 0.001 compared to control and ###p < 0.001 compared to Free siRNA.*